PB89-206684

Plume Dispersion in the Convective Boundary Layer
Part 1. CONDORS (CONvective Diffusion Observed by Remote Sensors) Field Experiment and Example Measurements

(U.S.) Environmental Protection Agency, Research Triangle Park, NC

May 88

U.S. Department of Commerce
National Technical Information Service
NTIS

TECHNICAL REPORT DATA
(Please read Instructions on the reverse before completing)

1. REPORT NO. EPA/600/J-88/331	2.
3. REC	PB89-206684
4. TITLE AND SUBTITLE: Plume Dispersion in the Convective Boundary Layer Part I: CONDORS Field Experiment and Example Measurements	5. REPORT DATE
	6. PERFORMING ORGANIZATION CODE
7. AUTHOR(S): W. L. Eberhard, W. R. Moninger, and G. A. Briggs	8. PERFORMING ORGANIZATION REPORT NO.
9. PERFORMING ORGANIZATION NAME AND ADDRESS: Wave Propagation Laboratory, Environmental Research Laboratories, NOAA, Boulder, CO 80303; Atmospheric Sciences Research Laboratory, Research Triangle Park, NC 27711	10. PROGRAM ELEMENT NO. A119/A/01/03-6086 (FY-87)
	11. CONTRACT/GRANT NO. IAG AD13F2A251
12. SPONSORING AGENCY NAME AND ADDRESS: Atmospheric Sciences Research Laboratory--RTP, NC; Office of Research and Development; Environmental Protection Agency; Research Triangle Park, NC 27711	13. TYPE OF REPORT AND PERIOD COVERED
	14. SPONSORING AGENCY CODE EPA/600/09

15. SUPPLEMENTARY NOTES

Journal of Applied Meterology, Vol. 27, No. 5, Mary 1988, pp. 599- 616

16. ABSTRACT

The dispersion of plumes of passive tracers in highly convective boundary layers was measured during late summer in 1982 and 1983. The 300-m tower of the Boulder Atmospheric Observatory supplied meteorological data and served as the platform for elevated sources. The parameters in convective scaling theory were determined, and extensive information on wind statistics was gathered. Mixed layer height was a consensus of determinations from the vertical extent of remotely sensed tracers, from on-site radiosonde profiles, and from lidar-observed gradients of the haze. The lidar measured the three-dimensional distribution of oil fog, and a radar similarly observed a plume of microwave-scattering chaff. Careful processing successfully removed interfering effects, such as attenuation of the lidar radiation and ground clutter in the radar signal. Although these tracers were not conserved, the profile shapes are trustworthy, and local downwind flux of measured concentrations was successfully applied in place of the release rate. However, any interpretation of the chaff data must consider the effect of gravitational settling. Two conservative gas tracers were also sampled on a single arc at the surface during the 1983 phase. A preliminary examination of the results indicates that the average vertical profiles are significantly non-Gaussian in shape in agreement with earlier laboratory and numerical simulations.

17. KEY WORDS AND DOCUMENT ANALYSIS

a. DESCRIPTORS	b. IDENTIFIERS/OPEN ENDED TERMS	c. COSATI Field/Group

REPRODUCED BY
U.S. DEPARTMENT OF COMMERCE
NATIONAL TECHNICAL INFORMATION SERVICE
SPRINGFIELD, VA. 22161

18. DISTRIBUTION STATEMENT: RELEASE TO PUBLIC	19. SECURITY CLASS (This Report): UNCLASSIFIED	21. NO. OF PAGES: 20
	20. SECURITY CLASS (This page): UNCLASSIFIED	22. PRICE: PC $13.95 / MF $6.95

EPA Form 2220-1 (Rev. 4-77) PREVIOUS EDITION IS OBSOLETE

EPA/600/J-88/331

Reprinted from JOURNAL OF APPLIED METEOROLOGY, Vol. 27, No. 5, May 1988
American Meteorological Society

Plume Dispersion in the Convective Boundary Layer. Part I: CONDORS Field Experiment and Example Measurements

W. L. EBERHARD AND W. R. MONINGER

Wave Propagation Laboratory, NOAA, Boulder, Colorado

G. A. BRIGGS*

Atmospheric Sciences Research Laboratory, USEPA, Research Triangle Park, North Carolina

(Manuscript received 30 June 1987, in final form 17 October 1987)

ABSTRACT

Project CONDORS (CONvective Diffusion Observed by Remote Sensors) measured the dispersion of a nonbuoyant plume in the highly convective boundary layer. Laboratory and numerical models have predicted vertical profiles of a passive tracer that are significantly non-Gaussian in shape in convective conditions. However, adequate field data to verify the model results were not available before CONDORS. A lidar measured the three-dimensional distribution of oil fog, and a radar similarly observed a plume of microwave-scattering chaff. The instrumentation, experimental methodology, and data reduction techniques are described. Analysis is still in progress, but preliminary results support most of the simulations, including the deviations of vertical profiles from Gaussian model predictions.

The experiment centered around the 300 m instrumented tower of the Boulder Atmospheric Observatory. The parameters in convective scaling theory were determined, and extensive information on wind statistics was gathered. Mixed-layer height was found by a consensus of determinations from the vertical extent of remotely sensed tracers, from on-site radiosonde profiles, and from lidar-observed gradients of the haze.

During the first phase in late summer of 1982, oil fog and chaff were released simultaneously either from the surface or from an elevated position on the tower. During the main phase a year later, the oil fog was usually released from the surface and chaff separately from the tower, and two conservative gas tracers were also sampled on a single arc at the surface. The use of multiple tracers permitted an evaluation of their performance. Careful processing of the remotely sensed tracer data successfully removed interfering effects, such as attenuation of the lidar radiation and ground clutter in the radar signal. Although these tracers were not conserved, valid profile shapes were obtained, and local downwind flux of measured concentrations was successfully applied in place of the release rate. However, any interpretation of the chaff data must consider the effect of gravitational settling. The three types of tracers complemented one another in revealing the dispersive behavior of plumes in convective conditions.

1. Introduction

The CONDORS (CONvective Diffusion Observed by Remote Sensors) experiment was designed to determine whether the non-Gaussian plume behaviors observed in laboratory and numerical simulations of dispersion in convective conditions actually occur in the atmosphere. These conditions dominate over land during most daylight hours, except during times of high winds, overcast skies, or snow cover. This experiment was carried out at the Boulder Atmospheric Observatory (BAO) of NOAA's Wave Propagation Laboratory during September 1982 and August–September 1983. Basic requirements not met by past field experiments were high quality meteorological measurements that include essential convective parameters such as the mixing depth, and vertical profiles of plume concentrations to heights of 1 or 2 km. Because of the latter requirement, two remote sensors were chosen to perform the primary tracer measurements: a lidar to map concentrations of oil droplets and a Doppler radar to map concentrations of aluminized chaff. The use of multiple tracer methods permitted an evaluation to substantiate their performance.

After a discussion of the experiment's background, subsequent sections of this paper describe the meteorological, lidar, radar, and surface sampler measurements, the scope of the dataset generated, and some example results. Kaimal et al. (1986) reported the experiment in greater detail and presented extensive tabulations of processed data. Additional preliminary analyses were presented in a series of conference papers (Moninger et al., 1983; Eberhard et al., 1985; Briggs et

* On assignment from the National Oceanic and Atmospheric Administration, U.S. Dept. of Commerce.

Corresponding author address: Dr. W. L. Eberhard, Wave Propagation Laboratory, NOAA, 325 Broadway, Boulder, CO 80303.

NTIS is authorized to reproduce and sell this report. Permission for further reproduction must be obtained from the copyright owner.

al., 1986). A later paper will report the conclusions from analysis of the entire dataset.

2. Experimental and theoretical background

Laboratory simulations by Willis and Deardorff (henceforth WD; 1976, 1978, and 1981) of dispersion in the convective boundary layer in a water tank produced vertical profiles of tracer concentration that deviated considerably from those predicted by conventional Gaussian plume models. Lamb (1978, 1979) obtained similar non-Gaussian distributions in numerical simulations of tracer trajectories using the turbulence field generated by the large-eddy simulation model of Deardorff (1974). Lamb (1978) also demonstrated the strong role of the large-eddy downdrafts and updrafts in creating the vertical distribution. These results have influenced many dispersion models: for instance, the parameterized alterations of Gaussian models surveyed by Briggs (1985), second-order closure models such as Sun and Chang's (1986), and Monte Carlo simulations such as Baerentsen and Berkowicz's (1984).

The simulations predicted that surface concentrations from an elevated release can exceed those from a surface release by a factor as large as 3 at certain distances downwind. For a passive tracer from a source near the surface, the maximum concentration first hugged the surface, and then lifted after a time of travel equal to about one-third the time it takes fluid in a typical thermal to rise to the top of the mixed layer. The concentration at the surface diminished rapidly with further distance downwind, as most of the material lofted into the upper-half of the mixed layer. At larger distances the material became more or less uniformly distributed throughout the depth of the mixed layer. In contrast to this, the maximum concentration of passive material from elevated souces descended until it reached the surface. Thereafter, it behaved in a manner similar to material released near the surface at the point of initial surface contact. The simulations showed significantly larger maximum surface concentrations from elevated releases than predicted by conventional Gaussian models.

Convective scaling theory (Deardorff, 1970) provides the foundation for analyses of the simulations and defines which meteorological measurements are essential in diffusion field experiments carried out during convective conditions, such as CONDORS. Weil (1985) cited the evidence for the validity of this scaling.

The mixed-layer height (z_i) scales the height (z) above the surface according to

$$Z = z/z_i. \tag{1}$$

The convective velocity scale is given by

$$w_* = (H_* z_i)^{1/3}, \tag{2}$$

where H_* is the surface buoyancy flux. Over surfaces that are not very moist, $H_* = (g/T)\overline{w'T'}$, where g is gravitational acceleration, T absolute temperature, w vertical velocity, and $\overline{w'T'}$ temperature flux (proportional to sensible heat flux) near the surface. The downwind distance x nondimensionalizes by

$$X = (x/\bar{u})w_*/z_i, \tag{3}$$

where $\bar{u}$ is the mean wind speed in the mixed layer. The ratio z_i/w_* is the characteristic time for a parcel to traverse about half the vertical extent of the mixed layer, and $x/\bar{u}$, is the transport time ($\bar{u}$ is normally nearly constant in the layer from 0.1 to $0.9z_i$). The crosswind distance (y) from the plume's axis scales by

$$Y = y/z_i, \tag{4}$$

and sampling duration time (t_s) by

$$\tau = t_s\bar{u}/z_i. \tag{5}$$

This time scale applies to Eulerian measurements because the size of the large convective eddies scales with z_i, and the eddies advect past a fixed point with speeds approximating $\bar{u}$.

In a field experiment designed to compare diffusion patterns with WD's laboratory results the ideal wind speed range must be chosen to minimize the effects of shear-produced turbulence and longitudinal diffusion. The laboratory tank had no mean flow and thus no wind shear. Concentrations were integrated over the horizontal dimension parallel to a line source, so longitudinal diffusion was inconsequential. The ratio of convectively generated to shear-generated turbulent kinetic energy is on the order of $(H_*/2)z_i/(\bar{u}u_*^2) \approx 0.1|z_i/L|$, where u_* is the surface friction velocity and L the Obukhov length. Thus, $-z_i/L$ must substantially exceed 10 for convectively produced turbulence to dominate and also to avoid organized convective rolls. According to Deardorff (1972), horizontal turbulence becomes fully isotropic when $-z_i/L$ equals or exceeds the order of 45. Since $-L$ increases rapidly with increasing wind speed, this consideration sets an upper limit on acceptable $\bar{u}$ values. Longitudinal diffusion becomes significant when $\bar{u} < 1.5w_*$ (Deardorff, 1975), which sets a lower limit. For the CONDORS site, considering the site roughness and typical midday values of H_*, Kaimal et al. (1986) estimated that the ideal range of $\bar{u}$ would be 2 to 6 m s^{-1} for the targeted z_i range of 500 to 1000 m.

3. Planning and performing the experiment

The 300 m tower (Kaimal and Gaynor, 1983) of the BAO served well as the site for CONDORS. Instrumented at eight levels, the tower supplied the required wind and turbulence measurements. The water tank simulations indicated an important dependence of dispersive behavior on nondimensional source height, given by

$$Z_s = z_s/z_i, \tag{6}$$

where z_s is the release height. Therefore, CONDORS included both surface and elevated releases of tracers. The tower's elevators carried the elevated-release tracer dispensers to z_s only minutes before they started an experimental run. We chose an elevated z_s according to the best estimate available of the midrun z_i and a desired value of 0.25 or 0.5 for Z_s.

a. *Two experimental phases*

The experiment consisted of two phases. The first phase during September of 1982 was primarily a test of the design concepts. The lidar measured the backscatter from a plume of oil drops. The radar similarly detected the return from microwave-scattering chaff. The tracers were released together so their measured concentrations could be compared for consistency. Half of the releases were elevated, and half were from the surface. Tracer measurements usually continued for 2 h near midday. Shorter periods comprising reasonably constant meteorological conditions and successful tracer measurements were later selected for analysis. We obtained tracer data for approximately 460 min distributed over 4 days, from which six periods totaling 226 min were processed.

The main phase followed during August and September 1983 with only minor changes from the first phase, except two gaseous tracers (SF_6 and Freon 13B1) were added. The measurements during the first phase of chaff concentrations near the surface releases proved to be unsatisfactory because the deposition rate was high, and terrain blocked the radar's view near the ground. Consequently, the chaff and SF_6 were released only from the tower during the second phase. The oil fog and Freon 13B1 were released at the surface, except for two runs with the oil fog colocated with chaff and SF_6. Simultaneous measurements of tracers with vertically separated release heights were intended to highlight the dependence of the plume's behavior on Z_s. We acquired tracer data for about 1080 min distributed over 8 days, from which 11 periods totaling 420 min were processed. Data from both phases can be integrated in the analysis.

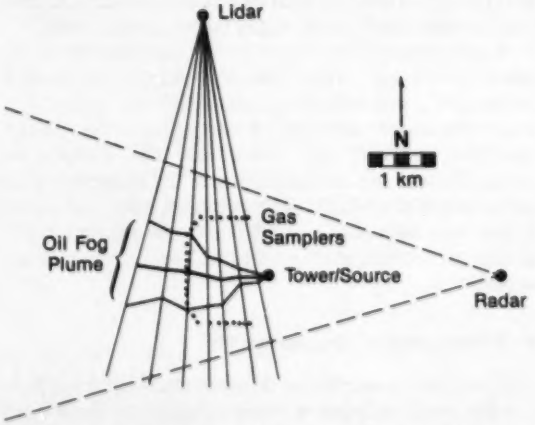

FIG. 1. Experiment layout and lidar scan planes during period 9–83 on 7 September 1983. The centerline and edges (10% of cross-sectional peak) of the vertically integrated oil fog plume averaged over the period are shown. The dashed lines delineate the azimuth limits of the radar scan. The dots show the locations of the gas samplers.

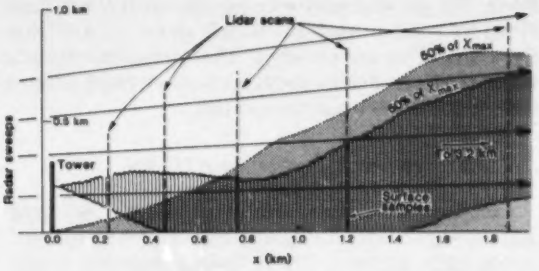

FIG. 2. Typical patterns for lidar scans and radar sweeps for the CONDORS experiments shown in relation to expected plume behavior. A surface release of oil fog and an elevated release of chaff are depicted. Note that x_{max} is the peak tracer concentration. The approximate location of the surface gas samplers is also indicated.

b. *Siting and scanning*

Figure 1 shows the 1983 deployment of the lidar, radar, and gas samplers. The lidar and radar mapped out the three-dimensional distributions of their respective tracers. From theoretical considerations and field experience, we concluded that interference between any of these tracers was negligible.

The pulsed lidar observed the oil fog plume by performing a repeating series of vertical scans in discrete planes at typically six azimuth directions, as illustrated in Figs. 1 and 2. One lidar scan cut across the north–south line of samplers during each 1983 run. Scans were mainly limited to values of x where the oil fog could be detected adequately, although we always attempted to reach to at least $X = 1$. The spacing between the scans increased with distance from the source.

The pulsed radar swept in azimuth at a repeating series of elevation angles. Figure 2 illustrates the discrete elevation angles, and Fig. 1 shows the boundaries of the azimuth scan for one case. The along-plume probing enabled the radar to quickly scan the distribution of chaff essentially throughout the volume of the plume to at least 3 or 4 km downwind of the source.

Figure 2 illustrates the philosophy behind the scan patterns of the lidar and radar and the location of the gas sampler arc. The distances of most interest in CONDORS spanned values of X between 0.3 and 1.2, where the maximum surface concentrations from elevated sources occur and where the deviations from Gaussian profiles are most likely. According to Eq. (3), this translates to $0.3 < x < 3$ km for the anticipated range of common meteorological conditions at the

BAO. The gas samplers were positioned at the surface along convenient roads in roughly an arc 1.2 km from the source. This was usually a little beyond the distance where the highest concentrations from elevated releases were expected to reach the ground.

c. *Convective climatology at the BAO site*

Archived tower data from 1979 to 1981 indicated that the experimental requirements were best fulfilled during early autumn. The following desirable conditions all occurred at 1300 MST on half the days during September of those years: sunny skies, wind speeds between 2 and 6 m s^{-1} at $z = 300$ m, and wind direction from the sector between 50° and 105°.

Cloudless skies were preferred because they allowed the maximum amount of insolation so that convection dominated the generation of turbulence. Any clouds originating from convection could disturb the capping inversion, cause reduced $\overline{w'T'}$ in shadowed areas, and contaminate the signals of the lidar and radar. Both phases were completed before the end of September because Denver and BAO records indicated increasing frequency of cloudiness in the following months.

Easterly winds were common during convective conditions, apparently because of thermally driven upslope winds toward the Rocky Mountains, whose foothills rise from the plains about 25 km to the west of the BAO. High wind speeds were undesirable for this study because mechanically generated turbulence would then become significant, invalidating convective scaling theory. At very low wind speeds, on the other hand, longitudinal diffusion becomes important, and the laboratory simulations would not be directly applicable. Low wind speeds also created operational problems when $\bar{u} < w_*$, causing the oil fog to occasionally move in the opposite direction of $\bar{u}$ toward both personnel and tower instrumentation.

The climatology of z_i was less well known. A few measurements made at the BAO during September 1978 indicated midday z_i values between 500 and 1000 m (Kaimal et al., 1980), an ideal range for the targeted source heights z_s at the surface, $0.25z_i$, and $0.5z_i$. Holzworth's (1972) climatology of mixing depths in the United States indicates much larger z_i over the high plains during spring and summer months.

Tracer measurements were performed near midday, when $\overline{w'T'}$ typically reached a maximum. (Solar noon is very close to 1200 MST at the BAO.) Generally, w_* peaked in the early afternoon, when the growth of z_i counterbalanced the decrease in $\overline{w'T'}$. Although the mixed layer earlier in the morning can be highly convective, the rapid fractional growth in z_i would have complicated the interpretation of tracer results. The late afternoon was also unsatisfactory, because z_i often grew rapidly after reaching an extended neutral layer and often scattered cumulus clouds developed. Tracer release began only after the easterly flow in the mixed layer appeared to be established. The earliest 2 h run commenced at 1025 MST, and the latest ended at 1515 MST.

The topography within 15 km of the tower is gently rolling. We believe the terrain variations did not appreciably channel the flow or affect large-scale turbulent eddies during convective conditions near midday. The surface cover of this rural area was principally long grasses with a few trees and building clusters scattered about. Surface roughness length for the CONDORS wind sector was approximately $z_0 = 3$ cm.

With easterly flow in the mixed layer, and prevailing westerly flow above, strong wind shear sometimes developed across the inversion. This shear caused the wind to turn with height within the mixed layer during some of the periods, which led to tilted shapes in the plume's cross section. The opposition of mixing layer and upper-level winds may also have caused an unusual amount of variability in wind direction.

d. *Daily operational strategy*

Preparation for a typical run began with a review of National Weather Service forecast maps the previous afternoon. The personnel entered a standby status when the outlook was favorable, which included clear to partly cloudy skies, synoptic high pressure at the surface, and light to moderate geostrophic winds. The radiosonde crew launched a balloon at the BAO near sunrise on a candidate day and tracked it to about 3 km AGL by double theodolite. According to these quickly processed profiles, which were supplemented by the 0600 MST sounding by the National Weather Service at Denver and by updated forecast maps, the participants decided whether to operate the equipment. During 1983 a numerical model for z_i growth (Wilczak and Phillips, 1986) assisted in this decision and helped forecast the best time to begin tracer measurements.

Wind speed and direction and z_i were closely monitored at the site. When favorable conditions seemed imminent, a run initiation time (RIT) was called. The tracer dispensers were raised into position and began operating about 15 min before the RIT. Lidar scan azimuths were selected according to the expected value of the length scale in (3). The samplers, lidar, and radar began data acquisition at RIT and continued for 2 h unless meteorological conditions deteriorated unacceptably.

4. Meteorological measurements

Tower instrumentation (Kaimal and Gaynor, 1983) at each level included a three-component sonic anemometer, quartz thermometer (for mean temperature), platinum wire sensor (for temperature fluctuations), and dewpoint hygrometer. Raw data were recorded at 10 Hz, which allowed later calculations of heat flux and various turbulence parameters for the analysis pe-

riods. The BAO computer printed in real time the most recent 20 min block averages of parameters like windspeed and direction, temperature, windspeed variances and covariances, and heat flux at each level.

Two or three rawinsondes were released during each tracer run to obtain the profiles of temperature, humidity, and wind above the tower. A radiometer measured the insolation.

The experimenters dedicated considerable effort to measuring z_i, which is the most important variable during convective conditions. The early growth of the mixed layer was monitored each experimental day by the tower's profile of temperature and humidity and by an acoustic sounder. Rawinsonde launches at about 0530 and 1000 MST, followed by the launches coinciding with the tracer measurements, were valuable in monitoring and predicting z_i. The lidar examined the vertical profile of haze, which usually exhibits a strong gradient at the capping inversion, and reported an estimated z_i every 20 min from about 1000 MST until the tracer run finished. The radar sometimes provided similar information on z_i based on scatterers presumed to be insects. The highest extent of the radar-observed chaff also helped reveal the depth of the mixed layer, to guide operations.

Figure 3 shows the data that guided selection of the analysis periods for the run of 7 September 1983. The wind data are 5 min averages from the tower's top levels, and heat fluxes are 20 min averages from the 10 and 22 m levels. The top frame shows estimates of z_i from lidar, radar, and rawinsonde data. The high radar observation at 1232 MST was probably from a very energetic thermal that penetrated the inversion. The lidar data indicate more frequent penetrations beginning about 1315 MST. The criteria for selection of an analysis period were least variability in z_i, $w_*/\bar{u}$, and wind direction θ_a. For instance, the rapid growth of z_i seen in Fig. 3 disqualified the data after 1350 MST. The large fractional change in $\bar{u}$ before 1230 MST was also unsatisfactory.

We determined $\bar{u}$ of the mixed layer for each analysis period by averaging the mean wind speeds from the 150, 200, 250, and 300 m levels of the tower. (Wind shear was usually negligible above 50 m.) The average of the mean wind directions from the same four levels produced $\bar{\theta}_a$. The average $\overline{w'T'}$ from the two lowest levels (10 and 22 m) provided the value of surface temperature flux. The probability distributions of wind azimuth and elevation angles at $z = 250$ m for each of the 11 analysis periods of 1983 were also extracted. Kaimal et al. (1986) report these data. Additional statistical information, too voluminous to include in the data report, was also calculated from the sonic anemometers. It is hoped these data can help demonstrate a direct connection between the nonisotropic turbulence and the nonsymmetrical profiles of the tracers.

The methods to determine mean z_i for each analysis period were more rigorous than those used in the period

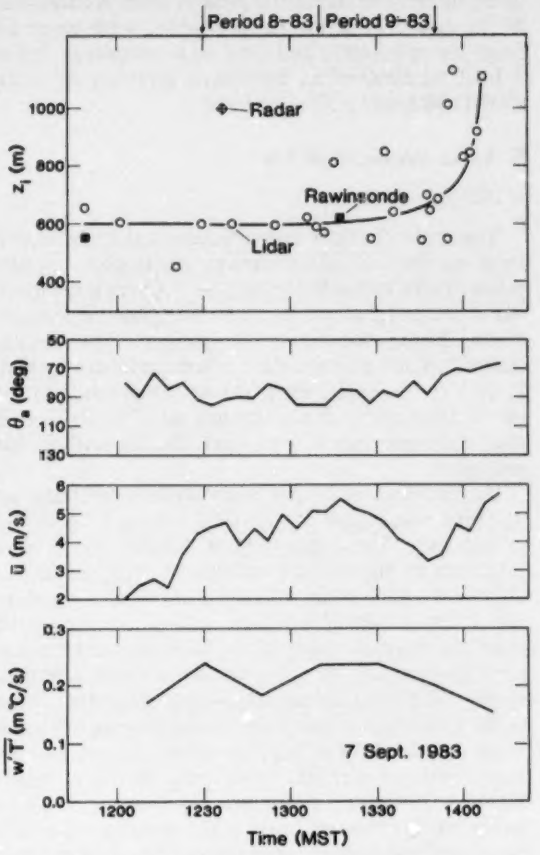

FIG. 3. Mixing depth, wind direction, wind speed and temperature flux versus time for the 7 September 1983 observing period (1210–1410 MST). Periods selected for analysis are indicated at the top. To a good approximation, $\overline{w'T'}$ of 0.1 m °C s^{-1} equals a sensible heat flux of 100 W m^{-2}.

selection process. The vertical profile of chaff or oil fog at a downwind distance sufficient for diffusion to the capping inversion provided an objective measure of z_i that corresponded with the upper profiles in the water tank simulations. For the 1982 data, the upper portion of the horizontally integrated profile of chaff was extrapolated to zero, and z_i was estimated as 0.92 times the height of the intercept. The results were consistent for, typically, $x > 2$ km. This method averages out much of the variation in the local inversion height associated with the random location and vigor of the thermal updrafts. We applied the same procedure to both the chaff and oil fog data for the 1983 data. (Oil fog profiles during 1982 did not extend far enough downwind.) However, not all of these profiles diminished smoothly to zero; some exhibited one or more steps, or even secondary peaks, near the top. In such cases, z_i was picked at the height where the horizontally integrated concentration dropped to 40% of the value

of the uppermost significant peak or shelf. A consensus of the results from the tracer profiles, with some aid from the radiosonde and lidar haze soundings, led to a final estimate of z_i. Estimated accuracy in z_i for CONDORS was ±50 m or better.

5. Lidar sensing of oil fog

a. Oil fog

The tracer for lidar measurement was a plume of a large number of light-scattering oil droplets, chosen primarily for its relatively low cost. (A very large number of scatterers are required for adequate lidar acquisition during convective conditions.) The foggers sprayed oil into a hot jet of air, where the oil evaporated. It then recondensed when it was exhausted into the cooler external air. Since virtually all of the drops had diameters less than 10 μm, gravitational settling was negligible.

On the basis of results from earlier brief tests, we operated one fogger during 1982 with a 35 g s^{-1} oil release rate. The fogger and its supply of oil were mounted on the tower's equipment carriage for elevated releases. Surface releases were from a location about 100 m west of the tower. Plume rise, calculated from the thermal energy of the fuel that fired the fogger's furnace, had an upper bound of 13 m. Unfortunately, the lidar could not adequately detect the plume as far downwind as had been hoped. During 1983 two foggers doubled the oil rate for surface releases, but the equipment carriage still could hold only one fogger. Signal acquisition was further improved in 1983 by switching to a heavier, lower vapor pressure oil, which evaporated more slowly after release. The median value of maximum X of only 0.61 for 1982 periods was increased in 1983 to 0.95 for elevated releases and 2.1 for surface releases.

b. Lidar data acquisition

The lidar revealed the concentration of the oil drops by measuring the fraction of transmitted light scattered back to a receiving telescope and detector. Eberhard and McNice (1986) described the lidar system; major points applicable to CONDORS are summarized here. The laser emitted 0.1 J pulses at 532.1 nm wavelength (green) and 10 Hz pulse rate. The receiver included a telescope with a 70-cm-diameter primary mirror, a 1.0 nm passband interference filter to reduce background light, and photomultiplier. Range resolution was 6 m (full width, half maximum), and beam divergence was 0.5 mr (full angle). The operator optimized the sensitivity of the system according to the peak signal in a scan by adjusting calibrated filters in the receiving optics. After linear, 8-bit digitization of the signal, usually at 3 m intervals in range, the data were recorded on digital magnetic tape for later processing.

Attenuation of the laser pulse by the oil fog dictated lidar scanning from the side of the plume. The lidar operator adjusted the elevation scan rate to obtain, roughly, 100 pulses in each scan. Scans were completed at typically 45 s intervals. Table 1 demonstrates that the spatial and temporal resolutions of the lidar measurements were fine. The sampling intervals in the vertical and cross-plume directions were also fine, but the downwind and temporal intervals were coarse.

c. Processing lidar returns

Although Eberhard et al. (1987) and Kaimal et al. (1986) explained the data processing procedures, we mention some aspects here as a foundation for discussing the data quality. The lidar equation for one pulse is

$$P(R) = K_L R^{-2}[\beta_p(R) + \beta_a(R)] \times \exp\left\{-2\int_0^R [\sigma_p(R) + \sigma_a(R)]dR\right\}, \quad (7)$$

where R is the range. The scatter from a diffuse, standard target determined the calibration factor K_L. Postprocessing solved the equation for β_p, which is the backscatter coefficient of the plume material. The backscatter coefficient β_a of the ambient haze (air molecules plus aerosol particles) created a contaminating signal that required removal. The exponential describes the attenuation of the pulse energy on its round-trip path to R. The extinction coefficient σ_p applies to the oil fog, and σ_a to the ambient haze. Interactive computer graphics aided in the extraction of $\beta_p(R)$.

In solving (7), we first applied the calibration and R^2 factors. The assumption of constant σ_a during each analysis period proved satisfactory. We determined its value by applying the slope method (Viezee et al., 1969) to a region without plume. However, σ_p was highly variable in time and space. The plume attenuation was determined by assuming a constant ratio,

$$S_p = \sigma_p(R)/\beta_p(R), \quad (8)$$

which is a rather stable property of the oil fog size distribution. This ratio was found from sample lidar pulses by investigating the amount of attenuation through the

TABLE 1. Typical tracer sampling resolutions and intervals.

Tracer Method	Vertical	Crosswind	Downwind	Time
Lidar				
Resolution	2 m	6 m	2 m	Instantaneous
Interval	10 m	3 m	380 m	210 s
Radar				
Resolution	70 m	160 m	90 m	Instantaneous
Interval	70 m	90 m	37.5 m	135 s
Gas				
Resolution	Point	Point	Point	Continuous
Interval	—	100 m	—	600 s

entire plume in situations where β_a could be assumed equal on opposite sides of the plume. Substitution of (8) into the lidar equation enabled correction for plume attenuation based on the measured signal alone. The plume in the scan closest to the source was sometimes optically dense enough to cause multiple scattering. The effect on the equivalent S_p was of secondary importance, so no compensation for multiple scattering was performed. We assumed β_a independent of range for each pulse, found its value in a region separated from the plume, and subtracted this value at all ranges. The interactive processing also permitted us to edit signals from high-voltage lines and to set β_p identically to zero in regions separated from the plume, especially at large R where the data became noisy.

The edited plume data were interpolated to rectangular grids in the scan planes, and scans in the same plane were averaged together. Grid spacing was 50 m $\times$ 50 m, although some data close to the source were also processed on a finer grid. The relative distribution of oil fog concentration became $\beta_p(\eta, z)$, where η is the horizontal distance from the lidar, and z is the height above the surface at the base of the tower.

The scan plane in general intercepted the plume at an angle different from the normal to the plume's horizontal axis. We projected the $\beta_p(\eta, z)$ data onto the normal plane to approximate the distribution in the cross section. The transform is

$$y = (\eta - \bar{\eta}) \cos\alpha, \tag{9}$$

where $\bar{\eta}$ is the centroid (i.e., first moment) of the horizontal profile, and α is the acute angle between the scan and projected planes.

d. Accuracy of oil fog concentrations

The size distribution of the oil fog was only poorly known, thus preventing an independent calibration of β_p versus oil mass. However, the assumption of uniform wind speed $\bar{u}$ within the mixed layer enabled us to calculate an empirical calibration factor K_o for the ratio of backscatter flux to oil release rate Q_o. The average amount of (conserved) tracer in a slab of unit thickness in the y–z plane is $Q_o/\bar{u}$. The total backscatter coefficient of tracer material is $\beta_p(y, z)$ integrated over the plane. Thus,

$$K_o = \bar{u}Q_o^{-1} \int\int \beta_p(y, z)dydz. \tag{10}$$

During 1982 the petroleum oil was a pale paraffin type, which we expected to behave somewhat like a conservative tracer. However, K_o declined substantially with distance downwind (Fig. 4). Gradual evaporation of the oil drops as the plume dispersed apparently caused most of the signal loss. Another factor in the decline of K_o with x may have been the loss of the more diffuse parts of the plume as they became undetectable against the noisy haze background. Deposition loss very likely had a minor effect. During some averaging periods the plume could not be clearly distinguished from the haze in many of the scans farthest downwind, so data in these scans were excluded from further analysis.

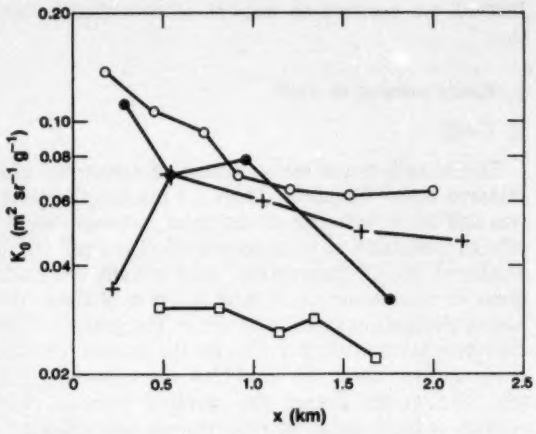

FIG. 4. Examples of the empirical normalization factor, i.e., the ratio of downwind flux of measured backscatter to release rate, for oil fog: Period 2–83 with a surface release of high-viscosity oil at a high rate (pluses); period 9–83 with an elevated release of high-viscosity oil at a moderate rate (circles); period 7–83 with an elevated release of high-viscosity oil at a low rate (squares); period 1–82 with an elevated release of moderate-viscosity oil at a high rate (filled circles).

An oil with higher viscosity and lower vapor pressure, which suffered less signal loss, was used in 1983. The decreased evaporation rate also made the oil fog detectable to a greater distance downwind.

Blockage by intervening terrain and safety restrictions prevented the lidar from measuring the plume all the way to the surface. The scan terminated anywhere from about 5 to 80 m above the ground, depending on the shape of the topography. Adjusted values for the partially scanned grid points of each vertical profile were calculated; Kaimal et al. (1986) list the heights of the lower cutoff. The scans closest to a surface release often missed a substantial fraction of the plume, which made K_o smaller, such as in period 2–83 (Fig. 4). Strong attenuation of the lidar's pulses by the plume in the plane nearest the source was sometimes undercorrected, which also diminished K_o. However, the shape of the time-average distribution was little altered, because in convective conditions it depends mainly on meander, which the lidar observed well even under strong attenuation. The gradient in the haze near z_i introduced some uncertainty into β_p in the top 10% or so of the mixed layer. The oil fog measurements were largely free of these problems away from the boundaries of the mixed layer and between the scan planes nearest to and farthest from the source.

Because loss of material was clearly indicated by the decline of K_o with distance, we did not attempt to use the actual oil release rate to normalize concentration.

Instead, we normalized with K_o as described in section 7.

6. Radar sensing of chaff

a. Chaff

The radar's tracer was a plume of numerous aluminized mylar filaments. Their 1.6 cm length, which was half the wavelength of the radar, provided highly efficient reflection of the microwaves. The chaff cutter produced 38 000 filaments s^{-1} and initially dispersed them in a small air jet. A large fraction of these filaments clumped together and fell to the ground. This clumping seemed most serious for the ground releases, presumably because the wind blew more strongly past the chaff cutter during the elevated releases. The clumps, which scattered microwaves less efficiently than single filaments, fell rapidly to the ground without significantly contaminating the data. The airborne filaments usually created adequate signal to at least x = 4 km.

Because the chaff had a terminal velocity of about 30 cm s^{-1}, gravitational settling cannot be neglected. However, the convective turbulence (characterized by typical w_* values of 1.8 m s^{-1}) was sufficiently strong to make the effects of the fall velocity relatively small. During all of the first phase of CONDORS, and two runs during the second phase, oil fog and chaff releases were colocated to examine how the settling altered the vertical distribution of the chaff.

b. Radar data acquisition

Moninger and Kropfli (1982) described radar procedures for an earlier demonstration experiment under conditions similar to CONDORS. During CONDORS the radar operated at a wavelength of 3.22 cm and a peak transmitted power of 20 kW. Range resolution was 90 m, and beam width was 0.8° (both full width, half maximum). The electronics averaged the signals from a number of pulses while the antenna swept in azimuth. The radar's dwell time for adequate accumulation of return signal was 324 ms, which made the horizontal (i.e., cross-beam) resolution typically twice the beam width. The logarithmic amplifier had a 70 dB dynamic range. Its output was digitized with 8-bit resolution at 37.5 m intervals in range and recorded on digital magnetic tape for later processing.

The insignificant attenuation of the microwaves by the chaff permitted along-plume probing, which enabled the radar to cover the region of interest more thoroughly than the lidar. The radar also measured Doppler shifts to obtain the speed of the chaff's motion parallel to the beam.

The operator adjusted the azimuth sweep rate to complete a scan of the entire volume of the plume about every 2 min. The steps in elevation angle were roughly equal to the vertical beam width. The temporal resolution of the radar data was essentially instantaneous. The spatial resolutions (Table 1) were adequate, except within a few hundred meters of the source. The spatial sampling interval was slightly finer than the resolution.

c. Processing radar returns

The average reflectivity of the chaff filaments, which were randomly oriented, could be calculated from their known dipole length. The chaff concentration N (in filaments m^{-3}) is given by (Schlesinger, 1961, p. 130)

$$N = \frac{\eta_c}{0.18\lambda^2}, \tag{11}$$

where η_c is the chaff's reflectivity, and λ the radar wavelength. Unlike the lidar, for which the tracer sizes were poorly known, the calibrated radar signal produced a direct measure of filament number density. However, the radar data also suffered some contamination.

A threshold on received power was applied to the data during post-processing to remove the receiver noise and exclude signals too weak to be reliable. The R^2 and calibration factors were applied next. Test signals applied to the receiver, along with the measurement of transmitted power, determined the calibration. The data were interpolated to a $(50\ m)^3$ Cartesian grid. The grid was rotated so that the x-axis lay parallel to the mean wind direction for each analysis period. The origin was positioned at the base of the tower. The orthogonal y-axis lay crosswind, and the z-axis was vertical.

Ground clutter (signal from the earth's surface, the BAO tower, and high voltage transmission line towers) created the most serious contamination of the chaff data. The nearby horizon at the radar site blocked the beam below about 0.5° and minimized the ground clutter in the vicinity of the plume. Most of the clutter in the data was removed by requiring the plume signal to exceed clutter data (which were recorded in the absence of chaff) by at least 10 dB. Some clutter remained at grid points adjacent to strong clutter. Since reflection from stationary objects has essentially zero Doppler velocity, most of this residual clutter was removed by requiring the velocity to exceed a threshold (typically 2 m s^{-1}) that depended on mean wind speed. A few remaining spurious data points, which were quite likely reflections from vehicles and aircraft, were discovered by inspection and removed manually.

d. Accuracy of chaff concentration

An empirical calibration factor to examine the characteristics of the chaff signal can be defined as

$$K_c = \bar{u} Q_c^{-1} \iint N(y, z) dy dz, \tag{12}$$

which is plotted in Fig. 5 for two periods. It shows the large degree of tracer loss due to clumping, because K_c would be unity for a fully conserved tracer. Much like the β_p data from the lidar, the most accurate N data from the radar occurred in the middle of the scanned volume. The steady drop in K_c beyond 1–2 km is probably due mostly to deposition losses of chaff resulting from its settling speed. Also, at larger distances, some diffuse parts of the plume fall below the processing threshold, and the depth of blockage increases from O(5%) of z_i near the tower to twice this at $x = 3.5$ km.

Data near the source had several difficulties. One was loss of plume information during removal of the clutter signal from the tower and its guy wires. Another was saturation of the receiver by the strong signal from the dense plume. These effects were apparent (Fig. 5) to, typically, $x = 0.6$ km. Blockage by terrain also caused the radar to miss much of the plume close to surface releases.

The blockage also prevented the radar from measuring tracer as close to the surface as the lidar could. The gradual nature of the radar's blockage prevented specification of a precise cut-off height for accurate data, but the processed returns generally show diminished concentrations below 60 m near the source and below 110 m at $x > 2$ km.

7. Normalization of remote sensor data

The trends in Figs. 4 and 5 demonstrate that the oil fog and chaff did not remain fully conserved. However, the point-to-point differences in K_o or K_c are partly caused by random variations in concentrations. Because of the dominance of large eddies, these differences may be appreciable in spite of the averaging of many scans.

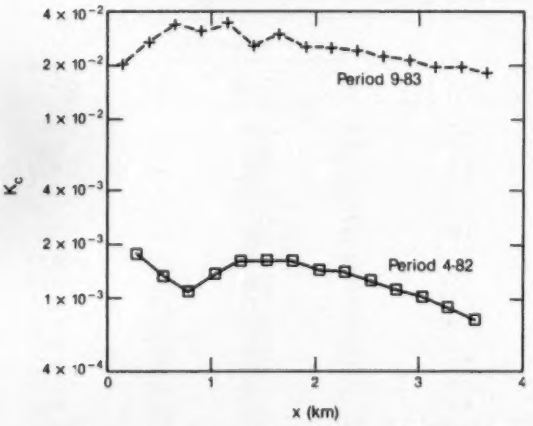

FIG. 5. Examples of the empirical normalization factor, i.e., the ratio of downwind flux of measured number concentration to release rate, for chaff. Release heights were 265 m for period 9–83 and 3 m for period 4–82.

We elected to normalize each β_p or N datum by the measured downwind flux of the tracer through the cross section containing the data point. This expedient assumes that the loss mechanisms were constant throughout each cross section. The expression for the oil fog is $\chi_o(y, z) = \beta_p(y, z)/K_o$ or

$$\chi_o(y, z)/Q_o = \beta_p(y, z) \Big/ \left\{ \bar{u} \int\int \beta_p(y, z) dy dz \right\}, \quad (13)$$

where χ_o is the mass load (g m^{-3}), and χ_o/Q_o is the dilution factor (s m^{-3}). The relationship for the chaff, where χ_c is the normalized number density (m^{-3}), is

$$\chi_c(y, z)/Q_c = N(y, z) \Big/ \left\{ \bar{u} \int\int N(y, z) dy dz \right\}. \quad (14)$$

Profile shapes for a tracer thus replaced absolute concentrations as the main basis for comparison. However, one can reverse the calculations with K_o and K_c to restore the measured values.

8. Surface sampling of gaseous tracers

The 1983 phase also included conventional gas tracers to provide a standard of comparison for surface concentrations inferred from the observed cross sections of the remotely sensed tracers. The gas tracers can be considered conservative. Since surface concentrations of the remotely sensed tracers required extrapolation from profiles above, surface sampling of the gases provided a valuable supplement. The release, sampling, and analysis of the gases were provided by NOAA's Air Resources Laboratory Field Office (ARLFO).

a. Sampling methodology

The SF_6 had a typical release rate of 0.2 g s^{-1} and was always adjacent (within a few meters) to the chaff release on the tower elevator. Freon 13B1 (CF_3Br), which was similarly released next to the oil foggers on the surface, had a typical release rate of 1.2 g s^{-1}. These rates were measured by a flowmeter and checked by the weight loss of the gas cylinder.

The samplers were arrayed (Fig. 1) approximately 1.2 km from the tower with straight legs parallel to roads for easy servicing, and with rounded corners near the road intersections. Angular separation from the tower was 5°, or roughly 100 m between samplers. Fill time for each of the 12 bags in each sampler was 10 min. A remote signal through a wire connected to all of the samplers initiated the 2 h sequences. The pumps cycled on and off each 5 s, so ingest could be considered essentially continuous. The ports were 0.6 m above the ground.

Absolute tracer concentrations χ_g in the bags were determined several days later at the ARLFO analysis laboratory in Idaho Falls by electron capture gas chromatography.

b. Accuracy of gas concentration

The anticipated accuracy in χ_g/Q_s for the SF_6, based on experience in other projects, was ±10% (Kaimal et al., 1986). The accuracy in 13B1 was considerably poorer, because the plume concentrations were of the same order as the analyzer's noise threshold.

Unfortunately, measurements for 3 of the 8 days of SF_6 sampling required rejection because of obvious, severe contamination. Measurements for all but one of the 5 days of 13B1 sampling were lost for the same reason (Kaimal et al., 1986). A thorough investigation by ARLFO revealed that the gas cylinder valves all leak to some minor extent; if the sampler bags are stored near the gas cylinders, especially in an enclosed space, the entrance tubing to the bags absorbs sufficient leaked gas to contaminate the analysis. Personnel failed to follow their instructions and placed partially used gas cylinders for transport to the analysis laboratory in the same truck as the bags from the last 3 experimental days. The contamination of 13B1 samples from 4 other days is believed to have been caused by storing bags near 13B1 cylinders at the BAO site, prior to use. The 13B1 samples from the remaining day were marginally adequate. The SF_6 samples from the remaining 5 days were quite satisfactory except for about 3% occurrence of "spikes" of unusually high concentration at single samplers. Although these spikes were very much smaller than the concentrations obtained for the contaminated sample days, they were large enough or persistent enough to suspect some additional contamination of unknown origin (Kaimal et al., 1986).

9. Scope and representativeness of the dataset

Table 2 lists basic information including convective parameters for each of the 17 averaging periods. Far more meteorological data, including 11 types of z_i estimates and frequency distributions of wind elevation and azimuth angles for each period, are given in Kaimal et al. (1986). That report also tabulates all uncontaminated 10 min and period-average χ/Q values for the gaseous tracers and includes extensive graphs and tables of oil fog and chaff data. Basic diffusion parameters, e.g., σ_y, σ_z, and mean plume height $\bar{z}$, are given as functions of distance for both tracers. For chaff, $\int \chi dz$ and $\int \chi dy$ distributions are tabulated up to $x \approx 3.6$ km. For oil fog, $\int \chi dz$ and $\int \chi dy$ are listed for each scan azimuth in each averaging period. Semiqualitative cross sections for χ for the oil fog in the two dimensions of each scan plane are shown, and χ/Q versus range and azimuth from the source is listed for the layer nearest the surface with complete lidar coverage.

Table 3 lists the medians and extremes of meteorological variables that are key to applying convective scaling theory to the 17 periods. For instance, the composite variable $z_i\bar{u}/w_*$ provides the nondimensional distance from the source according to (3). Thus, with a nominal maximum x of about 3.6 km, the upper limit on X for the chaff tracer ranged from 1.1 to 4.9, and measurements on the gas sampler arc were acquired for X between 0.4 and 1.6. The characteristic eddy passage time $z_i/\bar{u}$ varied almost an order of magnitude, which caused a wide range in the effectiveness of the periods as approximations to true ensemble averages.

We confirmed that the mixed layer was indeed very convective during all of the 17 periods by estimating

$$L = -u_*^3 T/(gk\overline{w'T'}), \tag{15}$$

where u_* is the friction velocity at the surface and $k \approx 0.4$ is the von Karman constant. The procedure for

TABLE 2. Meteorological averages and source summaries for CONDORS averaging periods.

Period number	Duration (min)	z_i (m)	$\overline{w'T'}$ (m °C s^{-1})	w_* (m s^{-1})	$\bar{u}$ (m s^{-1})	Source height* (m)			Elevated $Z_s = z_s/z_i$
						Oil	Chaff	SF_6	
0–82	36	1000	0.271	2.07	3.65	sfc	sfc	—	—
1–82	29	520	0.186	1.46	5.80	235	235	—	0.45
2–82	35	730	0.124	1.43	6.23	235	235	—	0.32
3–82	40	960	0.117	1.54	2.76	167	167	—	0.17
4–82	44	980	0.186	1.81	2.40	sfc	sfc	—	—
5–82	42	1260	0.148	1.82	1.59	sfc	sfc	—	—
1–83	30	1600	0.158	2.00	3.15	sfc	265	265	0.17
2–83	30	1240	0.207	2.01	1.91	sfc	235	235	0.19
3–83	60	1400	0.179	1.99	2.57	sfc	235	235	0.17
4–83	50	1100	0.189	1.88	1.90	sfc	280	280	0.25
5–83	40	880	0.152	1.64	2.52	280	280	280	0.32
6–83	30	880	0.184	1.74	2.59	280	280	280	0.32
7–83	30	880	0.158	1.65	3.34	280	280	280	0.32
8–83	40	640	0.130	1.38	4.45	265	265	265	0.41
9–83	40	780	0.133	1.48	4.59	265	265	265	0.34
10–83	30	900	0.200	1.80	2.09	sfc	235	—	0.26
11–83	40	870	0.227	1.86	1.57	sfc	235	—	0.27

* For underlined values, fully processed data are presented in Kaimel et al. (1986).

TABLE 3. Median and extremes of meteorological variables for the 17 periods processed from CONDORS.

Variables	Minimum	Median	Maximum
$\bar{u}$ (m s^{-1})	1.59	2.59	6.23
z_i (m)	520	900	1600
$\overline{w'T'}$ (m °C s^{-1})	0.117	0.179	0.271
w_* (m s^{-1})	1.38	1.80	2.07
$z_i\bar{u}/w_*$ (m)	734	1720	3180
$\bar{u}/w_*$	0.84	1.54	4.36
$z_i/\bar{u}$ (s)	90	349	792
$-z_i/L$	24	310	1125

determining u_* (Kaimal et al., 1986) was based on a simple wind profile law that fits well the Minnesota 1973 experimental data according to an unpublished analysis by Briggs. He found for $z \leq 0.2z_i$ that

$$u_* = k\bar{u}/\ln(z/z_0'), \tag{16}$$

where

$$z_0' = z_0(1 - 4z/L)^{0.6}. \tag{17}$$

These relationships were combined and solved for L by iteration using the $\bar{u}$ measurements at their average height of $z = 225$ m. In only two of the periods did the stability parameter $-z_i/L$ fail to reach or exceed 50. Periods 1–82 and 2–82 had $-z_i/L$ values of 29 and 24, respectively, which still indicates that convection was the most important source of turbulence. WD (1976) estimated that buoyancy causes the bulk of the turbulence when $\bar{u}/w_* \leq 6$. All CONDORS periods met this criterion.

The minimum limit on $\bar{u}$, to avoid significant longitudinal diffusion, was met less well. Half of the periods, all with $z_s/z_i < 0.3$, had $\bar{u}/w_*$ less than 1.5. This characteristic must be considered in comparisons with simulation results. However, the CONDORS dataset is fully valid for these low wind speeds and should provide valuable information on convective diffusion in such conditions, which frequently occur during the summer at some locations.

The multiplicity of tracers was an important design factor of CONDORS. A significant fraction of the experimental hours included colocated releases to allow a comparison of tracer performance. The sums of time for various combinations of colocated release are listed in Table 4. The time for each pair of tracers is in addition to that for the colocated trio of oil fog, chaff, and SF_6. These times can be compared with the total time for the 17 periods of 646 min.

We attempted during CONDORS to duplicate the nondimensional source heights Z_s of approximately 0, 0.25 and 0.5 that were used in the laboratory and numerical simulations. However, z_i proved difficult to predict accurately. The requirement for relatively steady meteorology and good data quality during each analysis period also happened to reduce the number of acceptable occasions when z_i growth caused Z_s to pass through a desired value. The partitions in Table 5 show that the source heights of the 17 CONDORS periods were mainly clustered at approximately 0, 0.18, 0.32, and 0.43. Interpolation methods will be required to compare CONDORS results with the earlier simulations.

The degree to which the CONDORS tracer data represent the average behavior for each Z_s must also be considered. Data should be acquired for a period long enough to average out the large looping and meander associated with plume dispersion in convective conditions. The data record must span a considerable number of eddy passages, i.e., $\tau_p \gg 1.5$, where τ_p is calculated according to (5). Willis and Deardorff (1976, 1978, and 1981) reported an equivalent τ_p of 28 for each Z_s (i.e., they averaged seven experiments using instantaneous line sources about $4z_i$ long). The CONDORS periods had a median τ_p of 6.6 and extremes of 2.8 and 19.4. Most of the individual CONDORS periods are too short to be considered representative. However, some of the periods with similar Z_s can be combined in the groups shown in Table 5 to achieve an acceptable nondimensional duration. We consider the totaled durations to be sufficiently representative of convective conditions for oil fog at $Z_s \approx 0$ (the chaff at this Z_s suffered too much blockage and deposition), chaff at $Z_s \approx 0.18$, and both oil fog and chaff, colocated, at $Z_s \approx 0.32$ and 0.43. The gas tracer measurements were made on only one arc, so are primarily useful for comparing with the inferred χ/Q of oil fog and chaff near the sampling arc during individual periods.

Ideally, the tracer concentration at each point should also be measured at least three times during the characteristic time for eddy passage to adequately sample the plume's vertical and horizontal meander. The nondimensional sampling interval, in terms of the $z_i/\bar{u}$ time scale, should then satisfy $\Delta\tau \leq 0.5$. This was not a problem for the continuous gas samplers. The lidar's sampling interval (Table 1) was typically 210 s. Since this gives $\Delta\tau \geq 0.5$ for half the periods, the effective representativeness of the lidar data was sometimes reduced. The radar also failed this criterion in about one-third of the periods. However, the radar's along-wind averaging considerably ameliorated the information loss.

10. Examples of results

Analysis of this whole dataset is not complete at this time, but several partial analyses have been presented

TABLE 4. Sampling duration for colocated tracer releases.

Tracer combination	Duration (min)
Oil fog and 13B1	30
Oil fog and chaff	190
Oil fog, chaff, and SF_6	180
Chaff and SF_6	170

TABLE 5. Sampling duration of tracers, segregated by approximate nondimensional release height Z_s.

	Duration					
	Dimensional time t (min)			Nondimensional time τ		
Z_s	Oil fog	Chaff	Gas	Oil fog	Chaff	Gas
<0.01	326	122	30	36.3	17.6	3.5
0.17–0.19	40	160	120	6.9	19.8	12.9
0.25	0	50	50	0.0	5.2	5.2
0.32–0.34	175	175	140	51.0	51.0	33.1
0.41–0.45	69	69	40	36.1	36.1	16.7
Total	610	576	380	130.3	129.7	71.4

in the data report (Kaimal et al., 1986) and in conference papers (Moninger et al., 1983; Eberhard et al., 1985; Briggs et al., 1986). Examples of these results are presented in this section. Because Z_s = 0.32–0.34 is the most well-represented case (see Table 5), with five periods of colocated oil fog and chaff releases and good SF_6 data coverage as well, it is chosen as our prime example. Longitudinal diffusion should be negligible during all the $Z_s \approx 0.32$ periods, as $\bar{u}/w_*$ ranged from 1.49 to 4.36. The value of $-z_i/L$ exceeded 50 in four of these five periods; it was estimated to be 24 in Period 2–82. One of these five, period 9–83, is used as an example for comparing oil fog and chaff $\int \chi dz$ and $\int \chi dy$ profiles at each lidar scan plane and for comparing SF_6 and oil fog χ/Q profiles near the surface. The wind direction was nearly directly from the east (87°) during this period, bringing the plume over the center of the sampling arc and permitting lidar scans all within ±10% of normal to the plume axis.

a. *Comparisons of horizontal profiles and σ_y*

We compared the concentration profiles of the simultaneously released tracers to verify the trustworthiness of their individual concentration patterns. Horizontal profiles of the vertically integrated concentrations $\int \chi dz$ of oil fog and chaff for period 9–83 are plotted against azimuth angle from the source in Fig. 6. Note that the distances x_L (lidar) and x_R (radar) of the y–z plane from the source are not identical in each frame. Also, the oil fog scan was perpendicular to the plume axis only at x_L = 717 m. The gross features of the oil fog profiles are consistent with those of the chaff, but the details differ. Such minor deviations are expected because of the patchiness of the plume and the lack of synchronization in time and space of the two instruments. The cruder lateral resolution of the radar is evident at x_R = 125 m, where it approximates the width of the reported chaff distribution (65°). Considering these differences, the horizontal profiles of chaff and oil fog are reasonably similar.

In Fig. 7, the lateral standard deviations σ_y of $\int \chi dz$ for all five periods of $Z_s \approx 0.32$ are plotted against distance, using the convective-scaling nondimension-

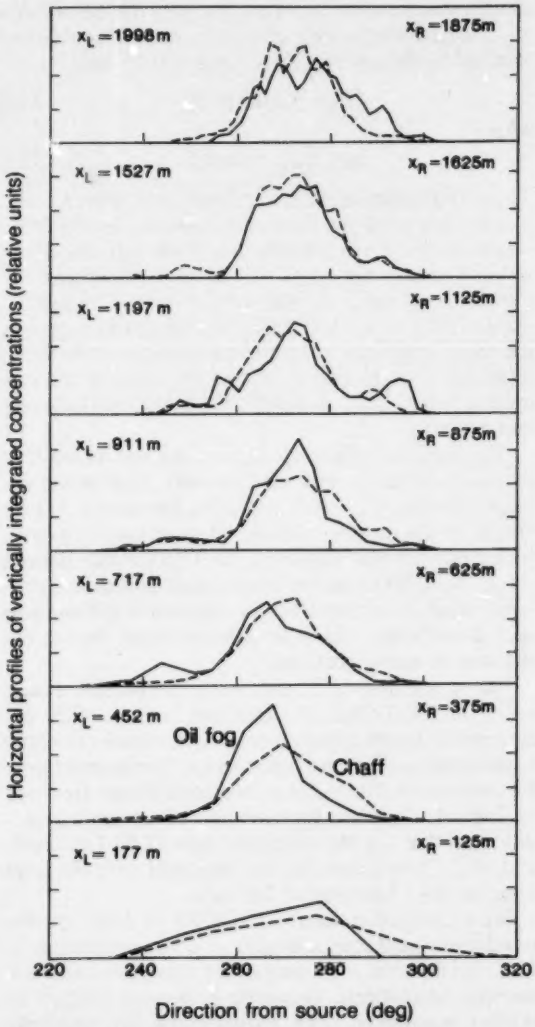

FIG. 6. Horizontal profiles of $\int \chi dz$ versus azimuth angle from source, for period 9–83: oil fog (solid line) and chaff (dashed line). Distance of the y–z plane from the source is x_L for the lidar and x_R for the radar.

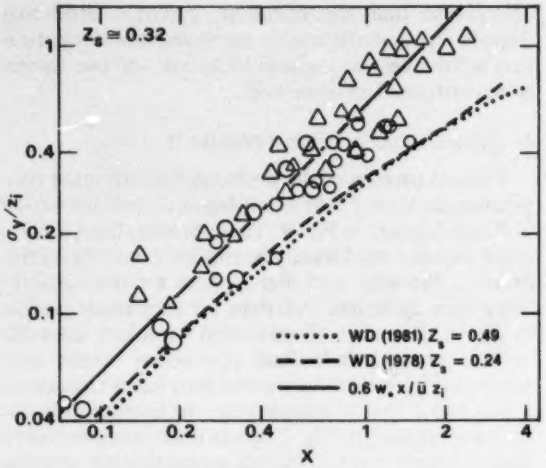

FIG. 7. Nondimensional lateral dispersion σ_y/z_i as a function of nondimensional downwind distance X for periods with $Z_s \approx 0.32$. The oil fog (circles) and chaff (triangles) are divided into two ranges of nondimensional period duration, 5.2–7.9 and 12.2–19.4, differentiated by the smaller and larger symbols, respectively. The dashed line shows the water tank results of WD (1978) for $Z_s = 0.24$, and the dotted line shows the WD (1981) results for $Z_s = 0.49$. The solid line is $\sigma_y = 0.6 w_* x/\bar{u}$.

alizations given by (3) and (4). Oil fog is represented by circles and chaff by triangles. The two symbol sizes indicate two ranges of dimensionless duration for each period. The smaller symbols apply to $\tau_p = 5.2$–7.9, and the larger are for 12.2–19.4. The median $(\sigma_y/z_i)/X$ of the smaller τ_p range is about 15% smaller than that of the larger τ_p range in Fig. 7. Much greater shortfalls in σ_y, on the order of 50% smaller than values from $\tau_p > 5.2$ periods, were seen in a third τ_p grouping (2.8–4.3), which occurred only in $Z_s \approx 0$ and 0.18, according to Briggs et al. (1986). They concluded that $\tau_p > 5$ is required for adequate averaging periods of σ_y in periods of quasi-steady state convective conditions. For $\tau_p = 5$, we crudely estimate σ_y averaging 25% smaller than our ideal average; for less than 10% shortfall, τ_p should be 10 or greater.

Our "ideal" average was of sufficient duration to encompass the passage of many (at least ten) individual thermals and downdrafts, with scales of the order of z_i, while avoiding large changes in z_i, $w_*/\bar{u}$, and θ_a. However, the goal of obtaining a true "ensemble" average in the sense of asymptotic values may be practically unattainable for σ_y in atmospheric convective boundary layers, because the outer limit of scales affecting horizontal motions reaches thousands of kilometers. On a typical convective day, air traverses several hundred kilometers, and on this scale there are usually many significant inhomogeneities in landform, land use, surface cover, surface moisture, evapotranspiration rate, etc. These all affect the local development of the convective boundary layer. Uneven development can cause unevenness in the horizontal flow field, so that a statistical steady state is never achieved as the atmospheric structure advects past a point. This may be one of the reasons we observe fairly abrupt wind direction or speed changes during most 2-h release periods, and usually obtained only 30 to 70 min of quasi-steady 5-min averages in the wind measurements. By choosing our averaging periods to avoid large wind changes that may be caused by large-scale horizontal inhomogeneities, we hoped to more closely approach the idealized conditions of the laboratory and numerical simulations we wish to test.

The oil fog σ_y values appear to be generally smaller than those for chaff in Fig. 7. Most of this difference can be attributed to the smaller fraction of chaff data in the smaller τ_p category. (This occurs because the contiguous periods 5–83 and 6–83 were combined during radar data processing.) At small X, much of the difference is due to the coarser lateral resolution of the chaff measurements. At large X, the lidar processing may have eliminated some of the outer edges of the oil fog plume because it was difficult to distinguish from the background haze. Overall, the measured σ_y values of oil fog are roughly 10% smaller than chaff values in comparable τ_p ranges.

Both chaff and oil fog σ_y values in Fig. 7 tend to be larger than those measured by WD (1978, 1981) in their laboratory tank experiments using elevated releases. They are about 40% larger than WD (1978, 1981) values in the lower half of the log$X$ range, a result consistent with Nieuwstadt's (1980) analysis of the Prairie Grass field data. (These data fell mostly in the range $0.01 < X < 0.4$.) Nieuwstadt attributed most of this difference to the effects of the tank walls, at $y \approx \pm 2z_i$, which restrict the formation of large (mesoscale) horizontal eddies. At $X > 1$, the field values tend to be about a factor of 2 larger than the WD (1978, 1981) values, and, in fact, approximately fit a simple linear relationship in x:

$$\sigma_y \approx 0.6 z_i X = 0.6 w_* x/\bar{u}. \tag{18}$$

This result is consistent with statistical theory for small x with the lateral velocity standard deviation given by $\sigma_v = 0.6 w_*$, which approximates many field-measured values of σ_v in convective boundary layers (Hicks, 1985). This result was also obtained for $Z_s \approx 0.43$ CONDORS data, but $Z_s < 0.2$ data were more consistent with the WD results (Briggs et al., 1986). We attributed the nearly linear behavior of σ_y in x for the $Z_s > 0.3$ releases to the unusually large directional wind shear in the upper part of the mixed layer at this site, resulting from the opposition of geostrophic and thermally driven upslope winds. However, Hanna (1986) recently obtained a result identical to (18) for surface SF_6 measurements extending to $x = 50$ km ($X \approx 20$) for a power plant in Indiana, albeit with much larger scatter than in Fig. 7.

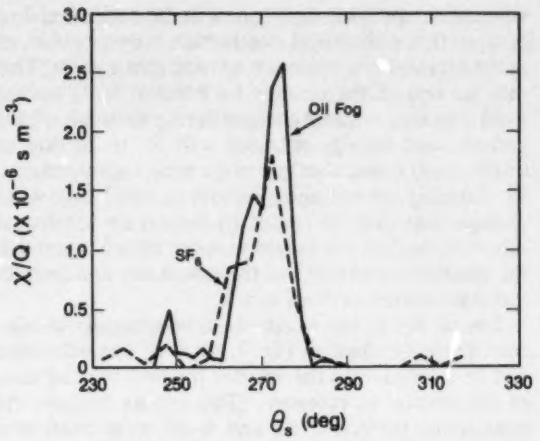

FIG. 8. Surface concentration distributions of SF_6 and oil fog nearest the sampling arc during period 9–83 versus azimuth from the source θ_s.

A comparison of oil fog and SF_6 dilution factors (Fig. 8) provided another check of the tracers. The lidar data came from the scan plane in Fig. 1 above the north–south leg of the sampler arc; this scan crosses the arc at a 3° angle, missing the northernmost sampler in the leg by about 20 m. Since the lidar could not scan completely to the ground, the surface concentrations of oil fog were assumed to be the same as those measured in a slightly elevated horizontal strip. The strip's vertical extent was 50 m, and its bottom edge about 22 m above the surface. A background value of 0.09×10^{-6} s m^{-3} has been subtracted from the SF_6 data. The integral of the oil fog profile in Fig. 8 is only 16% greater than that of the SF_6 profile. Considering the differences in the tracers, sampling and normalization techniques, and spatial locations, the two tracers were considered to agree well.

b. *Comparisons of vertical profiles, $\bar{z}$, and σ_z*

Vertical profiles of the horizontally integrated concentrations $\chi_y = \int \chi dy$ of oil fog and chaff for period 9–83 are plotted in Fig. 9. These profiles from a colocated release would ideally be similar. However, in this example the solid and dashed lines are only crudely alike; they agree less well than the horizontal profiles in Fig. 6. Period 9–83 produced especially irregular vertical profiles; individual convective events were poorly sampled by the remote sensor scans because $z_i/\bar{u}$ was only 170 s. In comparison, the profiles from the tank experiment in Fig. 9 reflect more complete sampling, a longer nondimensional sampling time, and also smoothing during processing (WD, 1978).

The mean height, $\bar{z}$, of the chaff distribution is noticeably lower than that of the oil fog in Fig. 9, except for a brief reversal at $X \approx 0.5$ (probably due to randomness and insufficient sampling). This height difference was a common feature of all colocated, elevated release periods. It can be mostly attributed to the effect of gravitational settling on the chaff. In Fig. 9, brackets within each frame indicate the vertical drop from release height resulting from a vertical speed -0.3 m s^{-1} times $x/\bar{u}$. Before chaff reaches the ground and reflection occurs, we generally find that this expected vertical drop is of the order of the observed $\bar{z}$ for chaff minus that for oil fog.

Except for the oil fog at $X \approx 0.5$ and the chaff at $X \approx 0.8$, the comparison of these profiles with the WD

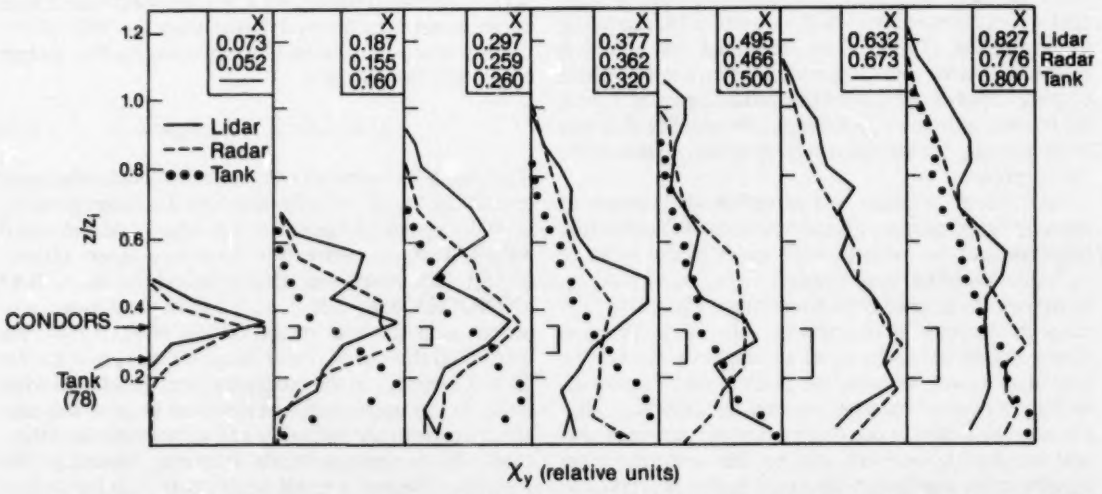

FIG. 9. Vertical profiles of $\int \chi dy = \chi_y$ in nondimensional coordinates. Oil fog (solid line) and chaff (dashed line) are from CONDORS period 9–83, and dots are from tank simulations (WD, 1978). Nondimensional downwind distances X for lidar, radar, and tank are shown at the top. The data at $X = 0.16$ for the tank are an average of results published for $X = 0.12$ and 0.20. Arrows along the ordinate indicate release heights, and brackets show vertical drop for a 0.3 m s^{-1} settling speed of the chaff.

tank profiles (1978) in Fig. 9 is not very favorable. However (as will be reflected in the surface concentrations shown in Fig. 12), it turns out that the vertical behavior of the plume during period 9–83 was atypical. It happens to be one of the two periods in 1983 in which the wind elevation angle near the release height was positive (upward) more often than negative (Kaimal et al., 1986; their Table 7.4). The consequence of this is reflected in the upward trend of the oil fog $\int \chi dy$ peak(s) seen in Fig. 9 at $X < 0.4$. The remaining nine periods in 1983 were dominated by negative wind elevation angles which was always reflected in the observed descent of the peak of the oil fog or chaff distributions in the short range from the source.

Figure 10 shows the behavior of $\bar{z}/z_i$ as a function of X for all the $Z_s \approx 0.32$ periods. In all cases for oil fog, and in half the cases for chaff, $\bar{z}$ at the smallest observed X was very near the actual release height, shown by a short horizontal line connected to the $\bar{z}/z_i$ point in question. At intermediate values of X, the scatter in $\bar{z}/z_i$ increased, and the chaff $\bar{z}$ was generally of the order of $0.1z_i$ below the oil fog's $\bar{z}$. Paradoxically, the oil fog $\bar{z}$ seems lower as $X \approx 1$ is approached, primarily because of two very low values at $X = 0.75$ and $X = 0.95$ from period 7–83. At these distances the oil fog $\int \chi dy$ profiles from this period indeed show marked peaks near the surface and very little material in the upper half of the mixed layer. In contrast, the chaff during this period went through a similar stage at $X \approx 0.4$ and then appeared to reflect upward, while the near-surface $\int \chi dz$ decreased to about one-fourth of its peak at $X \approx 0.8$. Similar, but less extreme patterns were seen during most colocated elevated releases: the chaff's peak in $\int \chi dy$ reached the surface before the oil fog's, while at larger X, the chaff diffused upward faster than the oil fog, probably assisted by earlier reflection from the surface. Beyond $X = 0.8$, Fig. 10 shows a remarkably consistent convergence of chaff toward the asymptote $\bar{z} = 0.5z_i$ for uniform concentration between $z = 0$ and z_i. These $\bar{z}/z_i$ values are also very similar to the WD (1978, 1981) results. Oil fog measurements do not quite extend to the distance where this asymptote

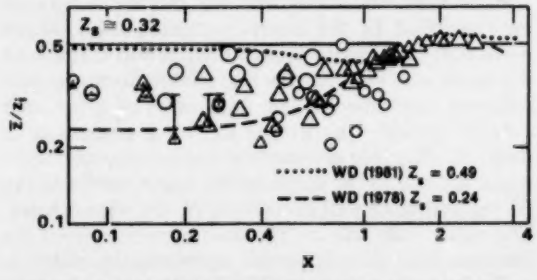

FIG. 10. Nondimensional mean tracer height $\bar{z}/z_i$ as a function of X for periods with $Z_s \approx 0.32$. Symbols and dashed and dotted lines as in Fig. 7 except the solid line is the asymptote for uniform vertical mixing to z_i. Vertical lines with a horizontal bar show release heights in relation to measurement closest to the source.

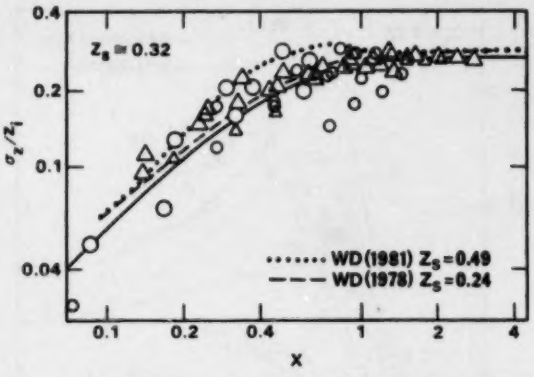

FIG. 11. Nondimensional vertical dispersion σ_z/z_i as a function of nondimensional downwind distance X for periods with $Z_s \approx 0.32$. Symbols and lines as in Fig. 7, except the solid line is $\sigma_z = 0.6w_*(x/\bar{u})/(1 + 5X^2)^{1/2}$.

is reached, $X \approx 1.7$, and show more scatter; part of this scatter may be due to the cruder sampling interval.

Figure 11 shows the behavior of σ_z/z_i for the same periods. There is much more consistency between oil fog and chaff σ_z measurements, compared with $\bar{z}$, and the scatter is remarkably small for field measurements. This result clearly shows the value of convective scaling to diffusion modeling. The data are also consistent with the results of WD's tank experiments (1978, 1981). Except for a few points with $\tau_p < 4.3$, which fell about a factor of 2 lower, Briggs et al. (1986) showed that σ_z from chaff and oil fog at *all* levels of release during CONDORS fit the simple equation

$$\sigma_z/z_i = 0.6X/(1 + 5X^2)^{1/2} \qquad (19)$$

rather well (Fig. 11), albeit with more scatter for the $Z_s \approx 0$ cases.

c. *Comparisons of surface* $\int \chi dy$

Concentration near the surface is of particular concern and needs to be modeled more accurately, if possible. For elevated sources, both WD's tank experiments (1978, 1981) and Lamb's numerical modeling (1978, 1979) indicated that conventional Gaussian models underpredict peak $\int \chi dy$ near the surface. This is confirmed by the CONDORS $Z_s \approx 0.32$ data plotted in Fig. 12, which includes SF_6 measurements on the sampling arc in addition to estimates from oil fog and chaff distributions. The direct chaff measurements were altered in two ways. First, blockage near the surface was compensated by multiplying the $\int \chi dy$ measured in the lowest layer (10–60 m) by the median ratio of lowest unblocked layer values to lowest layer values at $x > 2$ km, where concentrations were nearly uniform above the blocked layer. Chaff data were not used if this blockage factor exceeded 2, as it did in periods 2–82 and 7–83. Second, the effects of the 0.3 m s^{-1} settling speed on bringing the chaff to the surface faster than

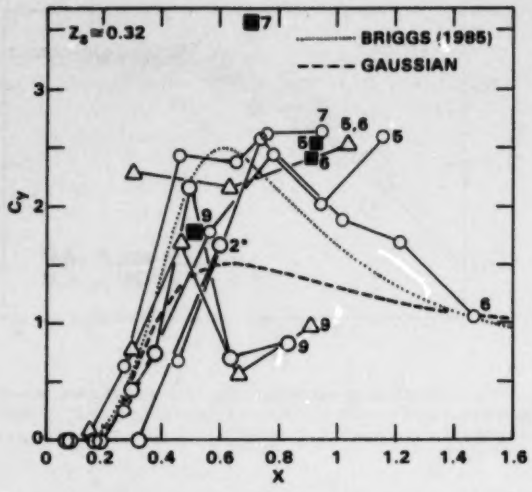

FIG. 12. Nondimensional crosswind integrated concentration near the surface, $C_y = \bar{u}z_i \int \chi dy/Q$, as a function of nondimensional distance X for periods with $Z_s \approx 0.32$. Symbols as in Fig. 7; in addition the filled squares are SF_6 measurements. Numbers identify periods, all in 1983 except for the asterisked period (1982). Corrections for blockage and settling velocity have been applied to chaff (see text). The dashed line is the Gaussian equation with $\sigma_z = 0.5w_*x/\bar{u}$, and the dotted line is Briggs' (1985) interpolation equation, which approximates WD (1976, 1978, 1981) tank results.

passive tracers was compensated by a simple scheme. The $\int \chi dy$ of the lowest layer (z = 10–60 m, or z_1 = 35 m at the middle) was moved from distance x out to a distance x' where it would have occurred had the chaff descended from the source height 0.3 m s^{-1} slower. It was also assumed that the plume underwent linear vertical expansion during this phase, so the $\int \chi dy$ transformed to x' was multiplied by x/x'. Such a simple scheme, which makes no assumptions about reflection or other diffusion mechanisms, cannot be expected to work at all distances. For instance, x' goes to infinity at $(z_s - z_1)\bar{u}/x$ = 0.3 m s^{-1} or $X = (w_*/0.3 \text{ m s}^{-1})(z_s - z_1)/z_i$, which is $X \approx 1.5$ in the case of Fig. 12 data. However, the scheme seems to work well near the distance of maximum surface impact.

Gaussian model predictions in Fig. 12 were calculated from the Gaussian equation with no reflection from z_i (reflection is significant only at $X > 1.4$) and using $\sigma_z = 0.5w_*x/\bar{u}$. (Near the source, $\sigma_z \approx 0.6w_*x/\bar{u}$, but diffusion toward the surface slows as the surface is approached, due to zero vertical velocity at $z = 0$.) A different assumption about σ_z growth would shift this distribution in X, but not in $C_y = \bar{u}z_i \int \chi dy/Q$. Clearly, conventional Gaussian models underpredict the peak $\int \chi dy$ in all cases. The WD results (1978, 1981) are not plotted directly because the different Z_s values result in shifts in both C_y and in X. To avoid this complication, an interpolation equation from Briggs (1985) that fits all the WD results is plotted for the case Z_s = 0.32. Most of the data fit this equation far better than the Gaussian model. Several period 9–83 points appear as anomalous, very low C_y values, probably in consequence of the unusual positive mode in wind elevation angle during this period, as discussed in section 10b in connection with Fig. 9.

11. Summary

The CONDORS field experiment produced a wealth of data on the dispersion of plumes of passive tracers in highly convective boundary layers. Meteorological measurements obtained ample information for applying convective scaling theory. Simultaneous release and measurement of as many as four independent tracers provided redundancy and detail on plume behavior. Two of these tracers were observed by remote sensors so that complete vertical profiles of concentration could be obtained; these were needed to meet a primary goal of verifying laboratory and numerical simulations that indicated that very non-Gaussian vertical concentration profiles develop during convective conditions.

The project centered on the 300-m BAO tower, which is located in gently rolling rural terrain. Tower instrumentation monitored the wind, turbulence, and sensible heat flux. Nearby radiosonde releases provided supporting measurements to above the mixed layer, which was 0.5 to 1.6 km deep during the experimental runs. These data were available immediately to guide decisions on tracer release. Lidar and radar profiles of naturally occurring scatterers also yielded real-time observations of z_i growth. These data were later used to select averaging periods for analysis based on the criteria of data completeness and reasonably steady meteorological conditions during each period.

Data were collected for a total of about 26 h during 12 midday runs in the late summers of 1982 and 1983. Almost 11 h divided into 17 averaging periods were selected for processing. Stability parameters showed that turbulence conditions ranged from moderately to extremely convective during the analysis periods ($-z_i/L$ = 24 to 1125). Tabulations of meteorological and tracer data for each averaging period appear in Kaimal et al. (1986).[1]

Basic wind, turbulence, and heat flux measurements were supplied by the tower instrumentation. Much more statistical information on wind and turbulence was processed than has been available from previous diffusion experiments. The final value of z_i for each analysis period was determined by a consensus of methods. The primary method was an objective technique applied to the shape of the upper profile of the oil fog and chaff well downwind of the release point. The radiosonde and the plume-free profiles from the lidar and radar gave important corroborating evidence.

The primary tracers in CONDORS were measured remotely by lidar and radar to observe their vertical

[1] Arrangements can also be made with one of the authors (Briggs) to obtain a copy of the dataset on floppy disk.

profiles. An elevator on the BAO tower was the platform for elevated releases, and a point a short distance from the tower's base was used for surface releases. A pulsed lidar measured the distribution of oil drops in cross sections of the plume at typically six distances downwind of the source by scanning in vertical planes from a vantage point to the side of the plume. A radar measured the concentration of microwave-scattering chaff from a location upwind of the source by scanning throughout the plume's volume to about 4 km or more downwind of the source. The radar data were transposed to Cartesian grid cells during processing. Gas tracers (SF_6 and 13B1) were sampled during the 1983 phase on an arc approximately 1.2 km from the source and near the anticipated region of peak surface concentrations from elevated releases. These tracers were intended primarily as checks on the χ/Q values inferred from the distributions of oil fog and chaff, neither of which are considered to be conservative.

Careful processing of the lidar and radar data achieved unusually good accuracy for these techniques. Lidar data on backscatter from the oil fog were corrected for the effects of attenuation and backscatter by the ambient haze and also for the frequently strong attenuation by the plume itself. Attenuation was not a problem for the radar, but extensive effort was required to successfully remove the strong signals from ground clutter. The sensitive radar-chaff technique usually performed well to at least 4 km downwind of release. The chaff's terminal fall velocity of about 30 cm s^{-1} is significant enough to require correction during analysis, but did not restrict the vertical mixing of the undeposited chaff. The oil drops are excellent tracers of air motion. Very good spatial resolution was obtained on the lidar scan planes, but the oil fog could not be detected as far downwind as the chaff. Oil fog concentrations were obtained, typically, only in six discrete planes.

The processed remote tracer data possess sufficient cumulative durations, in terms of $z_i/\bar{u}$, to represent ensemble averages for the release heights $z_s/z_i \approx 0$, 0.18, 0.32, and 0.43. Data at $z_s/z_i \approx 0.25$ are marginally useful. Because neither the chaff nor the oil fog was a conservative tracer, local downwind fluxes of measured concentrations were used in place of release rate to infer χ/Q. Examples presented here and elsewhere show good agreement between horizontal profiles of the chaff and oil fog downwind of a colocated release. Similarly, the oil fog concentration about 50 m above the gas samplers agreed well with SF_6 from a colocated release. As expected, the vertical profiles of chaff and oil fog agree less well; the differences are in qualitative accord with the gravitational settling of the chaff. Within the limitations described here, we have confidence in the accuracy of the profiles of oil fog and chaff.

Examples of comparisons of oil fog and chaff diffusion parameters with WD's (1978, 1981) tank simulation results were shown for $z_s/z_i \approx 0.32$, which is the nondimensional source height best represented by CONDORS data (five periods of colocated releases). The results for σ_z, $\bar{z}$, and near-surface $\int \chi dy$ were in good agreement with the tank results, when nondimensionalized in terms of convective scaling. The CONDORS σ_y was somewhat larger than in the tank and tended to be linear in x, approximating $0.6w_*x/\bar{u}$. Constraint of horizontal meander by the tank's walls and the large directional shear at the inversion during CONDORS were factors in the difference in σ_y, but their relative importance is not yet clear.

Study of the CONDORS data is still in progress, and results of comparisons with simulations and other field data will be published later. The discrepancy in σ_y is one of the issues under examination. However, preliminary assessments of the CONDORS profiles support the concept of convective scaling for atmospheric diffusion in convective conditions. The CONDORS data also support most results of laboratory and numerical simulations, including significant deviations of vertical profiles from Gaussian model predictions.

Acknowledgments. We thank NOAA's Air Resources Laboratory Field Office for the gas tracer measurements. The energetic contributions of the many individuals in the lidar, radar, radiosonde, gas tracer, and tower crews is appreciated. J. E. Gaynor, S. W. Troxel, and T. Uttal performed much of the data processing. J. C. Kaimal gave very helpful guidance and encouragement. This project was funded in part by the United States Environmental Protection Agency under Interagency Agreement AD13F2A251.

REFERENCES

Baerentsen, J. H., and R. Berkowicz, 1984: Monte Carlo simulation of plume dispersion in the convective boundary layer. *Atmos. Environ.*, **18**, 701–712.

Briggs, G. A., 1985: Analytical parameterizations of diffusion: The convective boundary layer. *J. Climate Appl. Meteor.*, **24**, 1167–1186.

——, W. L. Eberhard, J. E. Gaynor, W. R. Moninger and T. Uttal, 1986: Convective diffusion measurements compared with laboratory and numerical experiments. *Preprints Fifth Joint Conf. on Applications of Air Pollution Meteorology*, Chapel Hill, Amer. Meteor. Soc., 340–343.

Deardorff, J. W., 1970: Convective velocity and temperature scales for the unstable boundary layer for Rayleigh convection. *J. Atmos. Sci.*, **27**, 1211–1213.

——, 1972: Numerical investigation of neutral and unstable planetary boundary layers. *J. Atmos. Sci.*, **29**, 91–115.

——, 1974: Three-dimensional numerical study of the height and mean structure of a heated planetary boundary layer. *Bound.-Layer Meteor.*, **7**, 81–106.

——, 1975: A parameterization of diffusion into the mixed layer. *J. Appl. Meteor.*, **14**, 1451–1458.

Eberhard, W. L., and G. T. McNice, 1986: Versatile lidar for atmospheric studies, including plume dispersion, clouds, and stratospheric aerosol. *J. Atmos. Oceanic Technol.*, **3**, 614–622.

——, G. T. McNice and S. W. Troxel, 1987: Lidar sensing of plumed dispersion: Analysis methods and product quality for light-scattering tracer particles. *J. Atmos. Oceanic Technol.*, **4**, 674–689.

——, W. R. Moninger, T. Uttal, S. W. Troxel, J. E. Gaynor and G. A. Briggs, 1985: Field measurements in three dimensions of plume dispersion in the highly convective boundary layer. *Preprints Seventh Symp. on Turbulence and Diffusion*, Boulder, Amer. Meteor. Soc., 115–118.

Hanna, S. R., 1986: Lateral dispersion from tall stacks. *J. Climate Appl. Meteor.*, **25**, 1426–1433.

Hicks, B. B., 1985: Behavior of turbulent statistics in the convective boundary layer. *J. Climate. Appl. Meteor.*, **24**, 607–614.

Holzworth, G. C., 1972: Mixing heights, wind speeds, and potential for urban air pollution throughout the contiguous United States. U.S. Environmental Protection Agency Publ. AP-101, Research Triangle Park, NC 27711, 118 pp.

Kaimal, J. C., and J. E. Gaynor, 1983: The Boulder Atmospheric Observatory. *J. Climate Appl. Meteor.*, **22**, 863–880.

——, N. L. Abshire, R. B. Chadwick, M. T. Decker, W. H. Hooke, R. A. Kropfli, W. D. Neff, F. Pasqualucci and P. H. Hildebrand, 1980: Convective boundary layer thickness estimated by in-situ and remote probes. *Preprints Nineteenth Conf. on Radar Meteorology,* Miami, Amer. Meteor. Soc., 633–636.

——, W. L. Eberhard, W. M. Moninger, J. E. Gaynor, S. W. Troxel, T. Uttal, G. A. Briggs and G. E. Start, 1986: Project CONDORS: Convective diffusion observed by remote sensors. Boulder Atmos. Observatory Rep. #7, NOAA Wave Propagation Lab., Boulder, Colorado, [NTIS #PB 86-222 221/AS], 305 pp.

Lamb, R. G., 1978: A numerical simulation of dispersion from an elevated point source in the convective planetary boundary layer. *Atmos. Environ.*, **12**, 1297–1304.

——, 1979: The effects of release height on material dispersion in the convective planetary boundary layer. *Preprints Fourth Symposium on Turbulence, Diffusion, and Air Pollution,* Reno, Amer. Meteor. Soc., 27–33.

Moninger, W. R., and R. A. Kropfli, 1982: Radar observations of a plume from an elevated continuous point source. *J. Appl. Meteor.*, **21**, 1685–1697.

——, W. L. Eberhard, G. A. Briggs, R. A. Kropfli and J. C. Kaimal, 1983: Simultaneous radar and lidar observations of plumes from continuous point sources. *Preprints 21st Conf. on Radar Meteorology,* Edmonton, Amer. Meteor. Soc., 246–250.

Nieuwstadt, F. T. M., 1980: Application of mixed-layer similarity to the observed dispersion from a ground-level source. *J. Appl. Meteor.*, **19**, 157–162.

Schlesinger, R. J., 1961: *Principles of Electronic Warfare.* Prentice-Hall, 213 pp.

Sun, W.-Y., and C.-Z. Chang, 1986: Diffusion model for a convective layer: Part II. Plume released from a continuous point source. *J. Climate Appl. Meteor.*, **25**, 1454–1463.

Viezee, W., E. E. Uthe and R. T. H. Collis, 1969: Lidar observations of airfield approach conditions: An exploratory study. *J. Appl. Meteor.*, **8**, 274–283.

Weil, J. C., 1985: Updating applied diffusion models. *J. Climate Appl. Meteor.*, **24**, 1111–1130.

Wilczak, J. M., and M. S. Phillips, 1986: An indirect estimation of convective boundary layer structure for use in pollution dispersion models. *J. Climate Appl. Meteor.*, **25**, 1609–1624.

Willis, G. E., and J. W. Deardorff, 1976: A laboratory model of diffusion into the convective planetary boundary layer. *Quart. J. Roy. Meteor. Soc.*, **102**, 427–445.

——, and ——, 1978: A laboratory study of dispersion from an elevated source within a modeled convective planetary boundary layer. *Atmos. Environ.*, **12**, 1305–1311.

——, and ——, 1981: A laboratory study of dispersion from a source in the middle of the convectively mixed layer. *Atmos. Environ.*, **15**, 109–117.

NOTICE

This document has been reviewed in accordance with U.S. Environmental Protection Agency policy and approved for publication. Mention of trade names or commercial products does not constitute endorsement or recommendation for use.

This article documents research that was conducted under the auspices of the U.S. Environmental Protection Agency (USEPA). As an arm of the government, the USEPA has a paid up, non-exclusive, irrevocable, worldwide license to reproduce, prepare derivative works, and distribute to the public all of the material contained herein, and to grant others acting on its behalf the right to do so. The USEPA grants to the National Technical Information Service, Department of Commerce, the right to act as its agent in the distribution of this material.